2019-24-0033

Predictive CFD auto-tuning approach for an in-cylinder EU6 LDD DI engine

Author, co-author (Do NOT enter this information. It will be pulled from participant tab in MyTechZone)
Affiliation (Do NOT enter this information. It will be pulled from participant tab in MyTechZone)

Abstract

Tightening emission regulations and accelerating production cycles force engine developers to shift their attention towards virtual engineering tools. When simulating in-cylinder processes in commercial LDD DI engine development, the trade-off between run time and accuracy is typically tipped towards the former. High-fidelity simulation approaches which require little tuning would be desirable but require excessive computing resources. For this reason, industry still favors low-fidelity simulation approaches and bridges remaining uncertainties with prototyping and testing. The problem with low-fidelity simulations is that simplifications in the form of sub models introduce multi variable tuning parameter dependencies which, if not understood, impair the predictive nature of CFD simulations.

In previous work, the authors have successfully developed a boundary condition dependent input parameter table. This parameter table showed outstanding results for lab-scale experiments for over 40 varying operating conditions. The objective in this paper is first to identify the necessary considerations to adjust for the inherent differences between lab-scale and real engine conditions and then implement this parameter table into industry relevant conditions. With this approach the appropriate simulation setup for a real EU6 diesel engine can be predefined by the boundary conditions without previous tuning iterations. The performance of the simulation will be assessed based on its capability to match experimental heat release and chamber pressure data. The approach shown here has the potential to remove the necessity of lengthy tuning iterations and lays the groundwork for novel auto-tuned and predictive in-cylinder simulations.

Introduction

Emission regulations and shortening development cycles are putting increasing pressure on engine manufacturers. This development has led to a rising importance of early stage numerical simulations for in-cylinder processes. The simulation of a full cycle of a modern DI Diesel engine is challenging due to the multi-scale, multi-phase of the liquid-gas interactions and the numerical complexity of introducing finite-rate evaporation, mixing and multi-step reactions in the simulations. The available approaches to computationally resolve the underlying turbulent motion are in order of increasing runtime: Direct Numerical Simulation (DNS), Large Eddy Simulation (LES) and Reynolds-Averaged Navier-Stokes (RANS).

With current computational capabilities, an “all-scale” analysis of a single realistic engine case using DNS is nowhere close to being economically viable for commercial interest. In recent years, advancements in computational capabilities have made LES, which explicitly solves large eddies but implicitly accounts for small eddies with Sub Grid Scale (SGS) models, more accessible for some engineering problems, however not for problems with a wide range of geometric scales such as the modelling of IC engines. The fast RANS approach benefits from small runtimes and yields satisfactory results for most conventional commercial applications in the field of IC engines. In the RANS framework, turbulence is typically modelled by introducing additional transport equations and computes the Reynolds stresses using an Eddy-Viscosity term (turbulent viscosity). An averaged statistical approach to estimate various fluctuating quantities of interest are numerically triggered based on sub models. While the statistical averaging is the source of RANS’ low runtime, it is also the source of its high tuning dependency. To account for information lost at the sub-grid scale, sub models of varying degrees of fidelity are introduced to approximate a range of physical processes. Most of these sub models use user-definable parameters to encapsulate “unknown” or “unresolved” information at the sub grid scales.

It is common practice to set model coefficients for a specific case and then to use the same setup for multiple sets of boundary conditions. When following this approach, the key assumption made is that the simplified physics in the RANS sub-models, which are often developed at non-engine conditions, can adequately account for a change in turbulence levels, charge densities, temperatures and pressures as well as injection pressures without additional tuning. Previous work by the authors in [1, 2], where selected user-defined input parameters of a combination of sub models were varied and automatically optimized using a Design of Experiment (DoE) approach, [1] has shown that this assumption is problematic and usually leads to unsatisfactory results. It was shown that it is unlikely that a single combination of sub-models or coefficient matrix exists that can simulate the metrics of interest with acceptable accuracy. However, it was discovered that some simulation constants were sensitive to changing boundary conditions while others were not. Expanding on this finding, iterative optimization of the simulation setups for over 40 ECN Spray A conditions allowed the extraction of an input parameter matrix that matched experimental data of various comparison metrics like heat release, vapor & liquid penetrations, chamber pressures and mass fraction distributions. Further, and more importantly, the sensitivity of the input parameters could be linked to the governing physical processes at different conditions. This input parameter matrix works well for the lab scale ECN Spray A variations and it is the objective of this work to create a link to more realistic engine conditions.

Two load conditions, one part-load condition of a small bore LDD DI optical engine and one full-load condition of a EU6 LDD DI production engine, where experimental data is available, will be simulated using the tabulation derived from the ECN Spray A variations. The engines represent typical configurations that includes

a multi-hole injector, swirling ambient flow, large density, pressure and temperature gradients and moving geometry, all aspects not present in the ECN Spray A. It is therefore expected that some adjustments, primarily in turbulent air motion, will be necessary. The research questions for this work is therefore twofold:

1. How does the simulation setup derived from the Spray A tabulation perform under realistic engine conditions?
2. Which adjustments to the Spray A tabulation must be made to account for the different underlying boundary conditions?

To answer the above questions the paper will follow the following structure. The second chapter will introduce the experimental data for an optical engine from the ECN platform and acquired from in-house engine measurements of the EU6 LDD DI production engine and introduce the two operating conditions. The numerical setup is described in chapter 0. The methodology of how the simulation settings are derived from the previous ECN Spray cases is explained in more detail in chapter 0. Chapter 0 shows the results of the simulations against the experimental data and discusses implications on cylinder pressure, heat release and liquid penetrations.

Experimental Data

Engine configurations

For this study, two geometrically similar engines at two operating conditions were selected. The first engine is the ECN LDD small-bore engine, which the text will refer to as the optical engine. The experimental data was gathered by the Sandia National Laboratories and made accessible through the ECN platform [3]. It features a frequently used optically accessible General Motors 1.9L, single cylinder, light-duty engine (see [4-10]) which has been adapted from a production engine. This optical engine was selected because it offers an extensive dataset with measurements of liquid penetration and chamber pressure and offers images of combustion characteristics at part load conditions that resemble the ECN Spray A baseline at SoI. The engine offers this data at real engine operation with moving parts and steep thermodynamic state gradients. This is important to test the validity of the tabulation within the range of confidence before extrapolating into high load conditions.

The second engine is a EU6 LDD DI production engine without optical access. This engine will be referred to as thxe production engine. The experimental data for this engine is delivered from in-house measurements under full load conditions. The chamber pressure, density and temperature conditions all exceed the initial confidence range of the developed tabulation and therefore requires extrapolation. For this engine measurements time resolved global in-cylinder pressure and its derivative, the Rate of Heat Release (RoHR), are available. The engine configurations are listed in Table 1

Table 1: Engine specifications for the LDD optical and production engines

	Optical Engine	Production Engine
Bore x stroke (mm)	82 x 90.4	Similar*
Unit displacement (L)	477.2	
Geometric compression ratio (-)	16.7:1	
Cycle (-)	4-stroke	4-stroke
Intake/Exhaust valves (-)	2/2	2/2

*Confidential

Fuel injection equipment

In the optical engine the fuel was injected through a pre-production solenoid-based injector. A single injection of a blend of two Primary Reference Fuels (PRF) (more details below) is injected shortly after TDC with a rail pressure 800bar. The seven nozzles with a diameter of 139 µm are equally spaced around the mini sac. The included spray is 149˚. The production engine is fired with EU pump diesel injected through a similar multi-hole injector / nozzle configuration to the optical. A rail pressure of 1600 bar was used. More parameters of the FIE of both engines is listed in Table 2.

The optical engine was run with a blend of two PRFs named n-hexadecane and heptamethylnonane. The selection of this binary mixture was an attempt of achieving a simple 2-component diesel surrogate, whose liquid-phase physical properties and ignition properties were closer to those of a real Diesel fuel than those of a blend of n-heptane and isooctane which were used in previous studies [7].

It is important to mention that our simulations of this condition were conducted using reference Diesel. This was due to time constraints around building the appropriate fuel file. Running the simulations with reference Diesel, however, is still justifiable because the 2-component diesel surrogate was selected particularly because of its similarity of liquid-phase and ignition properties. We therefore expect minor uncertainties.

Table 2: Fuel injection equipment specifications

Injector specifications		
	Optical Engine	Production Engine
Nozzle diameter (µm)	139	Similar*
Number of holes (#)	7	
K-factor	1.5	
L/D	5.59	
Injection parameters		
Injection pressure (bar)	800	1600
Injected fuel mass (mg/cycle)	25.9	56.1
Start of injection (˚CA ATDC)	~2	~-11
Fuel	58 vol% heptamethylnonane (iso-$C_{16}H_{34}$) 42 vol% n-hexadecane (n-C_{16}-H_{34})	EU reference Diesel
Fuel temperature (°C)	90	150
Cetane number	50.7	

*Confidential

Engine operating conditions

The optical engine is run at a part load condition to protect the optical equipment. The boundary conditions at SoI strongly resemble the ECN Spray A baseline condition with a charge temperature of 900K and density of 22.8kg/m^3. The wall temperatures are controlled at 90 deg C. The engine is operated in a skip fired mode (fired every 5th cycle). The production engine represents a full load condition with a charge density and temperature at SoI beyond ECN Spray A. A full list of the operating conditions is provided in Table 3.

Table 3: Engine operating conditions and charge conditions at IVC and SoI

Engine Operating Conditions		
	Optical Engine Part load	Production Engine Full load
Engine speed (rpm)	1500	4000
Swirl ratio (Ricardo) (-)	2.2	Similar*
Wall temperatures (°C)	~90	~230
$IMEP_g$	9±0.1	
BMEP		17.6
Valve timings		
Intake Valve Closure (IVC) (˚aTDC)	-152	
Exhaust Valve Opening (EVO) (˚aTDC)	132	
Intake Conditions at IVC		
Intake charge mole fraction	19.7% O_2 79.2% N_2 1.1% CO_2	21% O_2 78% N_2 1% other
Intake gas flowrate (g/s)	8.51	143.2
Intake Pressure (bar)	1.51	2.86
Intake temperature (runner) (K)	353	423
EGR rate (simulated) (%)	10.3	0
Charge conditions at SoI (Calculated)		
Temperature (K)	~925	~1045
Density (kg/m^3)	~21.8	~32

*Confidential

Data acquisition

In the optical engine a Kistler 6125b pressure transducer mounted instead of the glow plug delivers a digitized pressure measurement at 0.25 ˚CA intervals. The ROHR is computed using an iterative two-zone model where the temperature and gas properties are considered. The heat release to the walls is deducted following measurements of motored cases. The ROHR of the production engine is estimated by post-processing the experimental in-cylinder pressure trace with the Rassweiler & Withrow method, which considers the pressure rises due to combustion and volume change. It assumes that the Mass Fraction Burned (MFB) is defined as the pressure rise being proportional to the heat added to the cylinder at every crank angle interval.

The optical engine allows optical access through fused silica windows (50 mm W x 25 mm H) at the top of the cylinder liner. Emission and cylinder pressure measurements were conducted using a classic titanium piston. For optical investigations the titanium piston was replaced by a fused silica piston. Geometric adaptation of the fused silica piston in comparison its titanium counterpart included a wider crevice and larger top land height facilitate the image acquisition at a minor effective compression ratio penalty. For a detailed summary of the used imaging techniques consult [5].

Numerical Setup

In this study, the focus of the work will lie on the simulation of the spray injection and combustion process. Therefore, port flow and intake stroke are not considered. The simulations will only investigate the duration between IVC and EVO. For this reason, the intake and exhaust ports have been removed and the valves shut. A full-geometry analysis is undertaken. The usual mesh and time-step independence studies were conducted to ensure model independence. Independence is found for a mesh size of 0.4x0.4mm (~250 000 cells for both engines) and a time step of 0.005CAs.

The study is conducted in Ricardo Software's commercially available CFD package VECTIS. It is a RANS based code with a long history of extensive industrial use for ICE's and is therefore well validated [11]. The used sub-models are largely industry standard and can be found in most other commercially available CFD solvers. This allows for the approach presented here to be applied on any other CFD package. The selected sub models are listed in Table 4.

Table 4: List of selected sub models

Turbulence Model	Standard k-ε [12]
Spray Injection Method	Blob (Single size)
Droplet Tracking method	Eularian-Lagrangian
Droplet Breakup Model	KH-RT with Levich switching criterion [13, 14]
Droplet Drag Model	Putnam [15]
Droplet evaporation	Spalding correlation [16, 17]
Phase interaction	Droplet-droplet & Droplet-turbulence (two-way coupling)
Auto Ignition Model	Livergood-Wu model [18]
Combustion model	Ricardo's Two-Zone Flamelet (RTZF) [19]
Laminar Flame Speed Model	Metghalchi & Keck model [20]
Turbulent Flame Speed	Gülder equation [21]

Methodology

The tabulation was derived in previous work by Nsikane *et al* in [1, 2, 22]. The methodology is in part inspired by the work done by Pei *et al* in [23, 24] and by benefits tabulated chemistry has proven to have over solving complex chemical reactions in terms of computational efficiency. Starting from the conditions of a simplified environment of constant volume experiments (ECN Spray A) [25], coefficient matrices that correspond to individual operating points were derived. These coefficient matrices are used to extract a mapping between the trend in the value change of these coefficients and the underlying physical conditions. The main findings in the previous work were:

- With an industry standard, RANS, Eularian-Lagrangian based CFD simulation software it was unlikely that a single combination of user definable constants could produce results that matched experimental data at various operating conditions.
- In previous work, the investigated operating conditions required no adaptation of the coefficients in the turbulence models. However, the investigated ECN Spray A cases did not include considerable combustion system modifications that allowed a closer study of the turbulence levels. It is expected that a combustion system that includes swirl and plume-to-plume interactions would require an adaptation of turbulence coefficients.
- The droplet drag scaling coefficient A_{drag} and the auto ignition coefficient of the Livengood-Wu model C_{ig} were found to be the tuning parameters which were most sensitive to changing boundary conditions. When using the Putman drag model, which assumes spherical droplets throughout fuel injection, the A_{drag} coefficient was necessary to reduce drag effects by accounting for droplet deformation. The auto-ignition coefficient links the complexity of the fuel specific ignition delay process with the simplistic Livengood-Wu auto-ignition model. The behavior of how to best set these values for a range of boundary conditions appeared to follow physically justifiable trends which opens possibilities of extrapolation into other operating conditions.
- The initial droplet sizes were treated as an input variable rather than a boundary condition due to the lack of experimental data on their real sizes and shapes. The KH-RT breakup model could, without being altered, accurately simulate droplet breakup and evaporation under the proviso that the initially introduced droplets diameters were adjusted in line with the boundary condition. Leaning on the Patterson-Reitz droplet introduction method [26], a tabulation of droplet sizes based on the operating condition was derived. This tabulation followed the physical reasoning that droplet sizes are sensitive to the ΔP between nozzle and combustion chamber.

The simulation settings used to run the individual engine conditions are extracted from a table which lists the value of a boundary condition sensitive simulation constant against a variety of boundary conditions like charge temperature, pressure and density as well as injection pressure. The coefficients, which in the previous work had proven to be insensitive to a change of charge conditions, were carried over directly. An example of how the tabulation was used to derive the coefficient values is given in the next section.

Tabulation of model constants based on Design of Experiment and subsequent iterative optimization

The tabulation was derived based on over 40 parametric variations of ECN Spray A. Five of the key points were selected as DoE key points. At each of these DoE key points, 140 simulations with individual combinations of simulation constants defined by the DoE software were run and post-processed. By calculating the Root-Mean-Square-Error (RMSE) between experimental data and the simulations of the four key metrics of each simulation, a Stochastic Response Model (SPM) for that condition was built. An integrated optimizer used the SPM to minimize the trade-off between the errors of the individual metrics and returned a set of promising simulation settings. By manually exploring inherent similarities between the promising settings of the selected DoE conditions, some patterns were derived. Iterative exploration of these patterns into the non-DoE Spray A key points then yielded the complete tabulation. The tabulation is reached by running every key point and recording the used parameter. While the DoE was used to identify the influential factors and visualize the error response of each coefficient, manual refinement for every case was required. The final tabulation was extracted by recording the used parameters for each case that led to an acceptable match of all four comparison parameters. An example of the refined results is given in Figure 1. The drag scaling coefficient is recorded over the changing charge density and injection pressure. Each hollow circle represents a distinct Spray A key point. By extrapolating the tabulation (linearly for charge density and 3rd order polynomial for injection pressure), the setup for the full-load engine condition (hollow squares) are found. No sensitivity of the drag scaling factor was recorded for charge temperature.

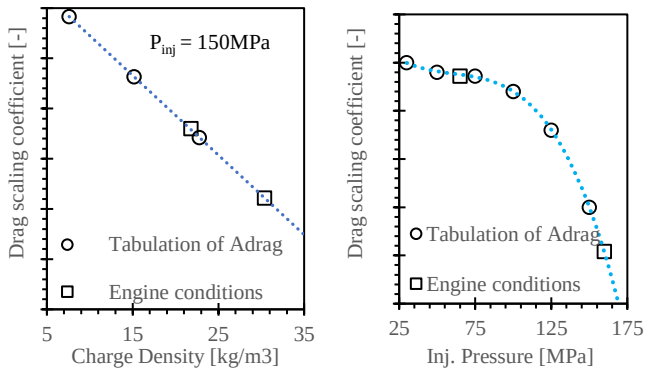

Figure 1: Tabulation of A_{drag} coefficient against charge density and injection pressure

Physical justification of tabulation

The high-pressure injection of fuel into a combustion chamber with elevated thermodynamic conditions can be roughly split in to two zones. The far-field, or dilute part of the spray where the fuel has evaporated and is mixing is well understood thanks to modern imaging techniques. The near-field, however, poses many challenges. Less well understood in-nozzle effects, sharp orifice pressure gradients and dense liquid injected at extreme velocities compounded with a lack of highly resolved imaging contribute to the computational models having difficulties accurately accounting for the governing physics. Large uncertainties around these types of flows persist around how to treat highly distorted droplet ligaments at nozzle exit. This brings in ambiguity how to represent droplet sizes and their drag with simplified sub-models. Here we have derived a method of scaling the near-field droplet drag coefficient and setting the initial droplet sizes as a function of injection pressure, gas density and temperature.

In previous work, the drag scaling coefficient A_{drag}, which is part of the droplet momentum calculation, was found to be one of the most influential tuning constants. The momentum equation for a droplet of mass m_d is described by Newton's Second Law ((1) in which C_d is the aerodynamic drag coefficient, A_f is the projected area of the droplet, A_{drag} is a user defined tuning coefficient, ρ_g is the density of the surrounding gas and the relative velocities between the droplets and the gas $\vec{U}$. This momentum contribution is then added into the energy and momentum conservation equations as a source term.

$$m_d \frac{d\vec{V}}{dt} = \frac{1}{2} C_d A_f A_{drag} \rho_g |\vec{U}| \qquad (1)$$

The drag coefficient C_d is calculated by the Putnam model, which stipulates that if the Reynolds number of the droplet is Re_d>1000, C_d is that of a sphere with a fixed value of 0.424. The assumption of spherical droplets goes against the consensus that droplets are more likely to leave the nozzle as highly deformed ligaments. Droplet deformation is thought to increase with increasing charge densities and injection pressures [27]. The drag scaling coefficient A_{drag} can reduce the drag coefficient by linearly scaling it. This means that while the droplet shape itself is not being adjusted (because it cannot if using the Putnam model), changing A_{drag} adjusts droplet drag and thus the liquid/gas momentum transfer as if the droplet were a ligament. Hence, although A_{drag} is not a physical coefficient per se, its adjustment certainly follows sound physical reasoning. Based on this, it has been hypothesized that a value of $0 < A_{drag} \leq 1$ in (1 is physically reasonable. Although values above 1 are numerically possible, they would not be physically justifiable.

Results and Discussion

The simulation setups for the two load conditions are derived from picking the simulation constants from different points in the tabulation. Two modifications had to be made to match peak pressure and heat release for both load conditions:

1. The turbulent Schmidt number had to be reduced to increase eddy diffusivity at high levels of stress that occurs at the early stages of injection.
2. The fuel vapor diffusion had to be increased by increasing the dissipation coefficient C_2 in the standard k-ε model.

The change of these two coefficients, which are both related to the mixing process between fuel vapor and the ambient air can be justified by the major difference between the ambient flow (ECN vessel ~0 swirl, LDD engines up to 2.2Rs) and plume-plume interaction (ECN Spray injector: single-hole, LDD engines: ~7-holes).

Cylinder pressure and heat release

Figure 2 shows the comparison between simulated and experimental in-cylinder pressures for both load conditions over crank angle. Directly carrying over the simulation setup from the Spray A setting derived from the tabulation results in an underprediction of peak cylinder pressure (orange/dashed line). The combustion induced pressure rise and peak cylinder pressure are better captured by the simulation with the turbulent Schmidt number S_t and raised the dissipation coefficient C_2 (blue/solid line). Minor discrepancies against the experimental data (black/dotted line) can be observed during the compression and, to a lesser extent, the expansion stroke. The improvement is significant in comparison to a simulation setup with the model settings left at default (green/dash-dotted line). The default setup appears to produce a good agreement for the part load conditions, but later analysis of the burn characteristics reveals shortcomings.

The RTZF combustion model calculates the enthalpies of formation from change of absolute enthalpy to change in total sensible enthalpy. The total heat release is derived from heat release contributions in every given timestep from the difference in formation enthalpies based on the conditions in every computational cell, the inlet/outlet boundaries and the compensation due to cooling effect from the spray. The final heat release is then a result of these contributions over the time-step size. This heat release is compared to the heat release derived from the respective engine pressure traces. Since they were obtained at different institutions and follow different post-processing routines and both methods differ from the way VECTIS calculates its heat release, only a qualitative comparison is possible.

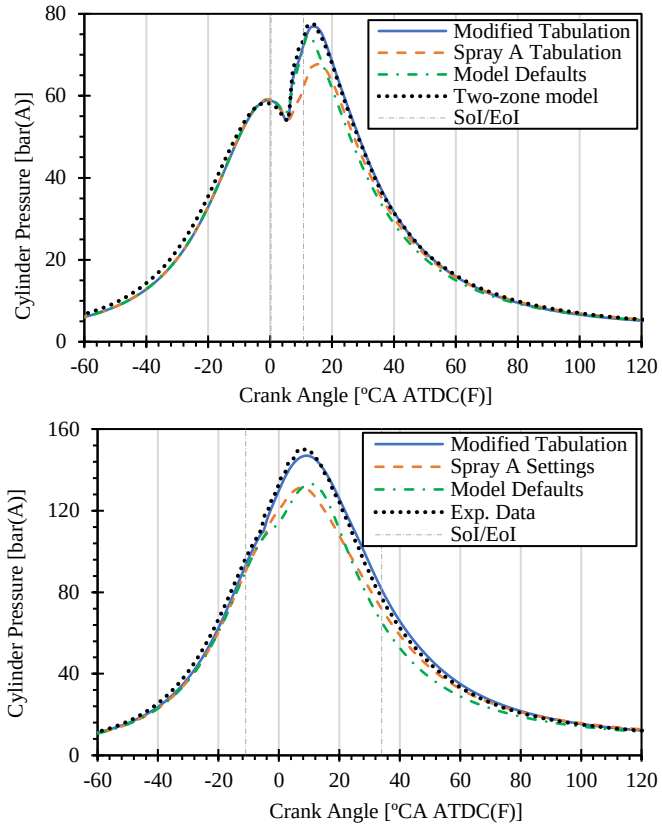

Figure 2: Comparison between simulated and experimental averaged charge pressure over crank angle

Figure 3 shows a comparison between the RoHR and Total Heat Release (THR) (black / dotted line) derived from the cylinder pressure trace and the VECTIS simulations using the "Spray A Tabulation" and its modification. In the case of the "Modified Tabulation" (blue / solid line), the Start of Combustion (SoC) and overall burn characteristics are captured well. For the production engine case some discrepancies can be seen at the peak and the transition into the tail of the heat release curve, indicating that some fuel that is not burned during the peak of the injection phase is burning later in the cycle. The original "Spray A Tabulation" (orange / dashed lines) shows a slow burn that extends throughout the expansion stroke. This was the main indication that the fuel mixing was occurring too slowly and had to be increased by modifying the turbulence coefficients. For both cases the ignition delay was well reproduced. The delay time allows for the fuel vapor to mix and reach the thermodynamic state at which it ignites. A slower mixing under less extreme conditions like the part-load condition allows for longer mixing time which then leads to a higher instantaneous heat release when the mixture eventually ignites. Under the high load condition, the threshold for ignition is crossed as the fuel is mixing. This produces a more progressive heat release, i.e. without the presence of a large premixed spike. Both these burn characteristics are presented in Figure 3. Again, a significant improvement with regards to a model setup following default model parameters (green / dash-dotted). For the optical engine combustion commences to early and too late for the production engine indicating that either the mixing is not occurring with the appropriate rates or the combustion

model is delay/advancing the combustion incorrectly. In both cases the heat release prematurely decreases sharply with a slow burn towards the end of the combustion.

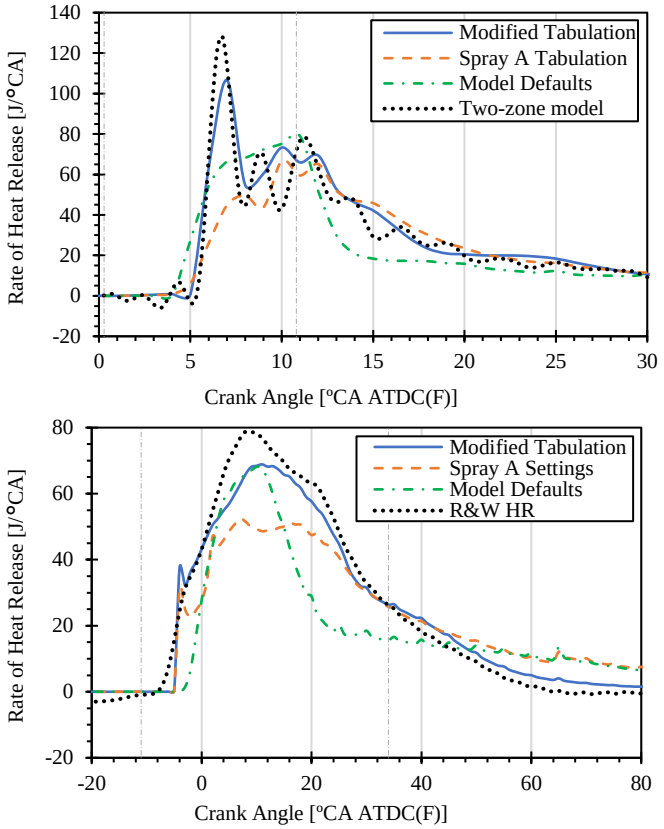

Figure 3: Comparison between simulated and experimental instantaneous heat release over crank angle

Liquid penetration

In Figure 4, time resolved spray tip penetration for both key points is plotted. For the optical engine experimental data for individual holes is available but has here been averaged. The simulated peak penetration and initial decline agrees well with the measuremnts. The shortening of liquid penetration between the "Spray A Settings" and the "Modified Tabulation" is attributed to the increase of the dissipation coefficient C_2. An increase of this parameter enhnaces turbulent mixing, which as stipulated by Siebers in [28], shortens liquid penetration due to the enhanced evaporation of droplets through exposure to more fresh hot ambient air. The increase in liquid penetration after the end of injection, which is indicated by the Rate of Injection (RoI) curve (gray dashed line) in Figure 4, is a result of very slow droplets being introduced into a cooling environment and appears under both load coniditions. These droplets of small but measurble mass linger and evaporate slowly rather than undergo traditional spray breakup due to aerodynamic effects. An increase in liquid penetration after the injection period can also be seen in the experiments which may be related to post injection nozzle dribble and droplet coalescence [29]. The slow evaporation and late combustion of these trailing droplets is the source of the elevated heat release towards the end of the combustion in Figure 3. These increases in liquid penetartion at the end of injection will be studied in more detailed in future work, but at this stage no connection between the two phenomena can be made.

Although there is no experimental data to compare to, the simulated liquid penetration of the production engine can give some indication about the evaporation of the fuel spray. The steady state liquid penetration of the simulation is ~6.4mm. An inert ECN Spray A condition at comparable charge temperatures and injection pressures, but with a lower charge density stabilizes at ~7.4mm. Increasing charge densities are one of the main factors for reducing liquid penetrations [30]. We remind the reader that the spray parameters of the KH-RT model are identical in both cases. The difference between the setups is that the tabulation suggests different initial droplet sizes and adjusted droplet drag to the condition. Due to the higher injection pressure and charge density, it is expected that the droplets introduced into the production engine are more distorted than those a optical engine. Therefore, in the production engine, the droplet drag coefficient A_{drag} is significantly reduced in comparison to the optical engine (see Figure 1).

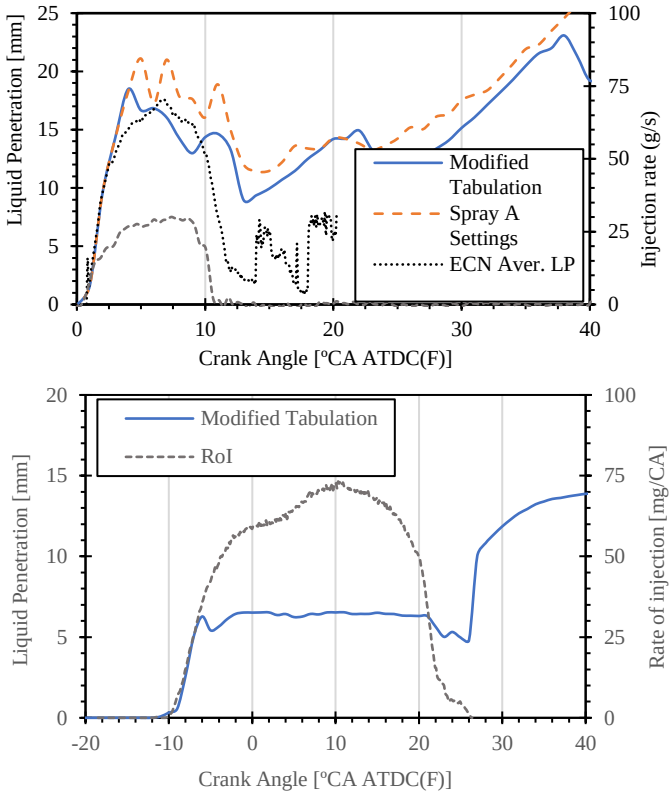

Figure 4: Liquid penetration and Rate of Injection over crank angle

Conclusions

For engine manufacturers to remain competitive they must keep up with the shortening development cycles and tightening emission regulations. To avoid lengthy prototyping and testing loops it is desirable to integrate virtual engineering tools like CFD into early stage engine development. To use simulation tools which resolve the full intake, compression, combustion and exhaust stroke of the cylinder down to the smallest scales would require enormous computational resources and would not deliver on the necessity of quick turnaround simulations that can compete with testbed data acquisition. For this reason, computation of turbulence has been typically performed with the RANS approach to keep runtimes acceptable. Other simplifications in spray breakup and evaporation,

combustion and emission simulations have led to the employment off sub models which require user intervention in form of input parameter tuning to deliver on accuracy. The plethora of available combinations of sub models and their associated input parameters makes simulation tuning a challenging task.

Our previous extensive assessment of the effect of combinations of simulation constants using Design of Experiments has indicated that there is no universally applicable simulation setup that can handle a variety of boundary (i.e. engine operating) conditions to an acceptable degree. To address this issue, previous work derived a tabulation of boundary condition sensitive simulation constants based on over 40 ECN Spray A parametric variations. This work expands this and investigates whether an input parameter matrix derived from this tabulation can be transferred from a lab scale to reproduce realistic engine test data. It is acknowledged that there are considerable differences between the Spray A configuration and a real engine case, hence it is anticipated that some parametric adjustments will have to be made. The conclusions are:

- Based on the tabulation derived under ECN Spray A conditions, the boundary condition sensitive simulation constants for the engine simulations are found via interpolation and extrapolation. The boundary condition insensitive simulation constants are carried over.
- The original "Spray A settings" cannot be directly transferred to the engine cases. The simulations estimate significantly reduced turbulent mixing by suppressing dissipating affects. While this may be appropriate for the governing conditions in the quiescent ECN combustion chamber, it does not represent the more turbulent conditions in the production engine. For this reason, the turbulent Schmidt number S_t and the coefficient of destruction of dissipation C_2 in the standard k-ε turbulence model must be adjusted.
- A "Modified Tabulation", which consists of the "Spray A Settings" with reduced turbulent Schmidt number S_t (increased eddy diffusivity) and increased dissipation coefficient C_2, performs well to replicate cylinder pressure, THR and RoHR at both load conditions. For both load conditions the dissipation coefficients C_2 were identical while turbulent Schmidt number S_t was slightly higher for the part load case.
- The liquid penetration of the optical engine shows good agreement to averaged experimental data. The increase of C_2 is thought to increases turbulent mixing. This in turn reduces the liquid penetration from the "Spray A Settings" to the "Modified Tabulation" setting. Inert simulations in previous work highlighted that the turbulent Schmidt number only has a minor effect on liquid penetration.

This novel approach shows good results for a tabulation guided setup of low-fidelity in-cylinder CFD simulations, which can be used to capture the main metrics of interest for engine development. Further investigations and refinement are necessary to adequately adjust for changing turbulence levels, as we progress toward the goal of removing iterative parameter tuning to enable fast and accurate simulations.

Contact Information

Daniel Nsikane
University of Brighton, Ricardo Innovations
d.nsikane@brighton.ac.uk
Daniel.nsikane@ricardo.com

Acknowledgments

The authors would like to acknowledge the high-quality experiments conducted the participants of the ECN, particularly the Sandia National Laboratories. VECTIS support was provided by Evgeniy Shapiro, Nick Tiney and Irufan Ahmed from Ricardo Software and nCal software assistance provided by Justin Seabrook. The authors would also like to thank the UK's Engineering and Physical Science Research Council support through the grant EP/P012744/1 and EP/S001824/1.

Definitions/Abbreviations

LDD DI	Light Duty Diesel Direct injected
CFD	Computational Fluid Dynamics
DNS	Direct Numerical Simulation
LES	Large Eddy Simulation
RANS	Reynolds-Averaged Navier-Stokes
ECN	Engine Combustion Network
ROHR	Rate of Heat Release
PRF	Primary Reference Fuel
FIE	Fuel Injection Equipment
$IMEP_g$	Indicated Mean Effective Pressure
IVC	Intake Valve Closure
EVO	Exhaust Valve Opening
EGR	Exhaust Gas Recirculation
SPM	Stochastic Process Model
BMEP	Break Mean Effective Pressure

References

[1] D. M. Nsikane, K. Mustafa, A. Ward, R. Morgan, D. Mason, and M. Heikal, "Statistical Approach on Visualizing Multi-Variable Interactions in a Hybrid Breakup Model under ECN Spray Conditions," *SAE International Journal of Engines,* vol. 10, no. 5, 2017.

[2] D. Nsikane, K. Vogiatzaki, R. Morgan, and M. Heikal, "Assessment of the performance of conventional spray models under high pressure and high temperature conditions using a "Design of Experiments" approach," presented at the ICLASS 2018, 14th Triennial International Conference on Liquid Atomization and Spray Systems, Chicago, USA, 2018. [Online]. Available: http://ilasseurope.org/events/iclass-2018/.

[3] S. Busch. "Engine Combustion Network - Small-bore diesel engine, https://ecn.sandia.gov/engines/small-bore-diesel-engine/." Engine Combustion Network. (accessed 27.06.2019.

[4] K. Zha, S. Busch, P. C. Miles, S. Wijeyakulasuriya, S. Mitra, and P. K. Senecal, "Characterization of Flow Asymmetry During the Compression Stroke Using Swirl-Plane PIV in a Light-Duty Optical Diesel Engine with the Re-entrant Piston Bowl Geometry," in *SAE International Journal of Engines* vol. 8, ed: SAE International, 2015, pp. 1837-1855.

[5] S. Busch *et al.*, "Experimental and Numerical Investigations of Close-Coupled Pilot Injections to Reduce Combustion Noise in a Small-Bore Diesel Engine," in *SAE International Journal of Engines* vol. 8, ed: SAE International, 2015, pp. 660-678.

[6] B. R. Petersen, I. W. Ekoto, and P. C. Miles, "An Investigation into the Effects of Fuel Properties and Engine Load on UHC and CO Emissions from a Light-Duty Optical Diesel Engine Operating in a Partially Premixed Combustion Regime," in *SAE International Journal of Engines* vol. 3, ed: SAE International, 2010, pp. 38-55.

[7] D. Sahoo, B. Petersen, and P. C. Miles, "Measurement of Equivalence Ratio in a Light-Duty Low Temperature Combustion Diesel Engine by Planar Laser Induced

Fluorescence of a Fuel Tracer," in *SAE International Journal of Engines* vol. 4, ed: SAE International, 2011, pp. 2312-2325.
[8] I. W. Ekoto *et al.*, "UHC and CO Emissions Sources from a Light-Duty Diesel Engine Undergoing Dilution-Controlled Low-Temperature Combustion," in *SAE International Journal of Engines* vol. 2, ed: Consiglio Nazionale delle Ricerche, 2009, pp. 411-430.
[9] D. Sahoo, P. C. Miles, J. Trost, and A. Leipertz, "The Impact of Fuel Mass, Injection Pressure, Ambient Temperature, and Swirl Ratio on the Mixture Preparation of a Pilot Injection," in *SAE International Journal of Engines* vol. 6, ed: SAE International, 2013, pp. 1716-1730.
[10] P. C. Miles, D. Sahoo, S. Busch, J. Trost, and A. Leipertz, "Pilot Injection Ignition Properties Under Low-Temperature, Dilute In-Cylinder Conditions," in *SAE International Journal of Engines* vol. 6, ed: SAE International, 2013, pp. 1888-1907.
[11] G. Li, S. M. Sapsford, and R. E. Morgan, "CFD Simulation of DI Diesel Truck Engine Combustion Using VECTIS," 2000. [Online]. Available: https://doi.org/10.4271/2000-01-2940.
[12] W. P. Jones and B. E. Launder, "The prediction of laminarization with a two-equation model of turbulence," *International Journal of Heat and Mass Transfer*, vol. 15, no. 2, pp. 301-314, 1972/02/01 1972, doi: http://dx.doi.org/10.1016/0017-9310(72)90076-2.
[13] A. Lefebvre, *Atomization and Sprays*. Taylor & Francis, 1988.
[14] J. C. Beale, *Modeling fuel injection using Kelvin-Helmholtz/Rayleigh-Taylor hybrid atomization model in KIVA-3V*. University of Wisconsin--Madison, 1999.
[15] A. Putnam, "Integratable Form of Droplet Drag Coefficient," vol. 31, ed: J. Am. Rocket Soc., 1961, pp. 1467-4798.
[16] S. D.B., "The Combustion of Liquid Fuels," presented at the 4th Symposium (International) on Combustion, Baltimore, 1953.
[17] J. S. a. L. Chin, A.H., "The Role of the Heat-up Period in Fuel Drop Evaporation," *Int. J. Turbo Jet Engines*, vol. vol. 2,, pp. pp. 315-325, 1985.
[18] J. C. Livengood and P. C. Wu, "Correlation of autoignition phenomena in internal combustion engines and rapid compression machines," *Symposium (International) on Combustion*, vol. 5, no. 1, pp. 347-356, 1955/01/01/ 1955, doi: https://doi.org/10.1016/S0082-0784(55)80047-1.
[19] C. Chen, M. E. A. Bardsley, and R. J. R. Johns, "Two-Zone Flamelet Combustion Model," 2000. [Online]. Available: https://doi.org/10.4271/2000-01-2810.
[20] M. Metghalchi and J. C. Keck, "Burning velocities of mixtures of air with methanol, isooctane, and indolene at high pressure and temperature," *Combustion and Flame*, vol. 48, pp. 191-210, 1982/01/01/ 1982, doi: https://doi.org/10.1016/0010-2180(82)90127-4.
[21] Ö. L. Gülder, "Turbulent premixed flame propagation models for different combustion regimes," *Symposium (International) on Combustion*, vol. 23, no. 1, pp. 743-750, 1991/01/01/ 1991, doi: https://doi.org/10.1016/S0082-0784(06)80325-5.
[22] D. Nsikane, K. Vogiatzaki, and R. Morgan, "Predictive Engine Simulations based on a novel DoE/RANS approach with coefficient tabulation," presented at the IMechE, Fuel Systems-Engines, London, 2018.
[23] Y. Pei, M. J. Davis, L. M. Pickett, and S. Som, "Engine Combustion Network (ECN): Global sensitivity analysis of Spray A for different combustion vessels," *Combustion and Flame*, vol. 162, no. 6, pp. 2337-2347, 6// 2015, doi: http://dx.doi.org/10.1016/j.combustflame.2015.01.024.
[24] Y. Pei, R. Shan, S. Som, T. Lu, D. Longman, and M. J. Davis, "Global Sensitivity Analysis of a Diesel Engine Simulation with Multi-Target Functions," 2014. [Online]. Available: http://dx.doi.org/10.4271/2014-01-1117.
[25] L. M. Pickett *et al.*, "Comparison of Diesel Spray Combustion in Different High-Temperature, High-Pressure Facilities," *SAE International Journal of Engines*, vol. 3, no. 2, pp. 156-181, 2010, doi: 10.4271/2010-01-2106.
[26] A. B. Liu, D. Mather, and R. D. Reitz, "Modeling the Effects of Drop Drag and Breakup on Fuel Sprays," 1993. [Online]. Available: https://doi.org/10.4271/930072.
[27] C. Crua, M. R. Heikal, and M. R. Gold, "Microscopic imaging of the initial stage of diesel spray formation," *Fuel*, vol. 157, pp. 140-150, 10/1/ 2015, doi: http://dx.doi.org/10.1016/j.fuel.2015.04.041.
[28] D. L. Siebers, "Liquid-Phase Fuel Penetration in Diesel Sprays," 1998. [Online]. Available: https://doi.org/10.4271/980809.
[29] D. Sykes, G. de Sercey, M. Gold, R. Pearson, and C. Crua, "Visual Analyses of End of Injection Liquid Structures and the Behaviour of Nozzle Surface-Bound Fuel in a Direct Injection Diesel Engine," 2019-01-15, 2019.
[30] J. D. Naber and D. L. Siebers, "Effects of Gas Density and Vaporization on Penetration and Dispersion of Diesel Sprays," 1996. [Online]. Available: http://dx.doi.org/10.4271/960034.